Proceedings of the Estonian Academy of Sciences,
2014, **63**, 1, 62–74
doi: 10.3176/proc.2014.1.09
Available online at www.eap.ee/proceedings

ENGINEERING

Comparison of the wear and frictional properties of Cu matrix composites prepared by pulsed electric current sintering

Riina Ritasalo[a*], Maksim Antonov[b], Renno Veinthal[b], and Simo-Pekka Hannula[a]

[a] School of Chemical Technology, Aalto University, P.O. Box 16200, FI-00076 Aalto, Espoo, Finland
[b] Department of Materials Engineering, Tallinn University of Technology, Ehitajate tee 5, 19086 Tallinn, Estonia

Received 28 November 2013, accepted 13 January 2014, available online 14 March 2014

Abstract. Wear performance of Cu matrix composites prepared by pulsed electric current sintering (PECS) was evaluated by using non-lubricated sliding tests. The studied materials contained cuprite (Cu_2O), alumina (Al_2O_3), titaniumdiboride (TiB_2) or diamond dispersoids in a coarse-grained Cu (c-Cu), submicron-grained Cu (sm-Cu), or nano-grained Cu (nCu) matrix. PECS compacted matrix materials were used as references. The ball-on-flat tests showed strong dependence of the coefficient of friction (CoF), wear rate and wear mechanism on the counter ball material. Cr-steel balls led to high CoF (0.71–1.01) and high wear rate (1.3×10^{-5}–5.7×10^{-3} mm^3/Nm) depending on the test material and its reactivity with the counterpart. Cu-Cu_2O yielded to lowest CoF and wear rate with a presence of oxidational and abrasive wear, whereas, Cu-Al_2O_3 and Cu-diamond suffered of adhesive wear leading to much higher wear rates. On the other hand, alumina ceramic counterpart led to a considerably lower CoF (0.39–0.92) and wear rate (1.4×10^{-7}–6.1×10^{-6} [mm^3/Nm]), and the test materials showed oxidational wear and material pile-up. Of the composites, Cu-diamond showed the lowest wear rate and Cu-Cu_2O and Cu-diamond (5 nm) showed the lowest CoF against alumina. It is believed that the present work gives new insights for materials selection, e.g., in electronic connector parts.

Key words: copper, Cu-composites, sliding friction, non-lubricated wear, spark plasma sintering (SPS).

1. INTRODUCTION

Copper has a wide range of excellent properties like high electrical and thermal conductivity, corrosion resistance and it is also well alloyable and has good joining characteristics [1,2]. The main drawback associated with Cu is its relatively low strength [1–3]. Dispersion strengthening (DS) with fine particles is one of the most suitable ways to increase the high-temperature strength of Cu [1,2], the method is also usable for modifying tribological properties [2,4,5]. Basically, Cu-based materials are developed for a wide range of applications like heat exchangers, structural parts, electrical connectors and contacts, e.g. brushes, as well as friction parts of machines, e.g., bearings and bushings [2,3,6,7]. The present study focuses on properties of Cu-based materials for electrical contacts and connectors, either in separable or permanent applications. Separable devices make and break electrical circuits several times during their lifetime and are designed for occasional or frequent insertions and removals [2,8]. Examples are contact points for resistance welding electrodes, electrodes generally, electrical switches, electrical brushes, and electrical switch gears and wires for electrical motors [2,9,10]. In permanent applications the wire terminations are fixed [8]. These are meant to be installed and left alone, and can be made by electrically and mechanically stable, e.g., solder joints. The application areas include computer, telecommunication, utility, aerospace, and automotive industries [8]. Since wear and friction coefficients represent interface stability and life of the contact under repeated cyclic motion, CoF may be used as an indirect measure of contact surface degradation affecting electrical signals quality [8].

Generally, a relative motion between the surfaces results in resistance to motion, i.e., friction, as well as progressive loss of the material by, e.g., abrasion, adhesion, chemical wear, and fatigue [3,4,6]. Abrasive

* Corresponding author, riina.ritasalo@aalto.fi

wear in the contacts results in scratching, furrows, work hardening, or grooves [3,4,6], whereas, adhesive wear causes a strong adherence between the asperities leading to separation in the bulk of softer material [3,6]. Fatigue wear occurs in cyclically stressed material surfaces, i.e., in bearings and gears [6], and chemical wear is detrimental chemical reactions in the contact influenced by environment in combination with mechanical contact mechanisms [6]. Oxidational wear is the most common chemical wear process [3,6], in which a thin oxide layer prevents the bonding between the asperities as well as metal–metal contact. The oxide can be a result of diffusion controlled oxide growth or agglomeration of oxide/oxidized debris/inclusion of oxide/oxygen into highly disrupted surface regions [11,12]. After critical thickness, it can lead to delamination at the metal/oxide interface [11–13].

Overall, wear control is challenging due to many factors involving, e.g., environment (temperature, humidity, oxygen content), contact (normal load, sliding speed, type of motion), and material properties (e.g., hardness, surface roughness, contaminations, porosity and interfacial bond of reinforcement) [3,6]. For Cu, the attemps to reduce wear and the friction force includes grain refinement [12–15], presence of oxide film/depris, tribolayer or mechanically mixed layer (MML) [5,12–14,16–20], as well as alloying, and DS [4,5,19–23]. The tribological behaviour of nano- and coarse-grained Cu has been studied in [12–15]. It was shown that in ball-on-disk oscillating tests with 5 N load against WC-Co balls the wear loss was four times higher for c-Cu (coarse-Cu) than for nc-Cu (nano-Cu), the respective CoFs being 0.74 and 0.54. However, the difference became less with higher loads [12]. It was also shown that the c-Cu worn subsurface consisted of a deformed layer with refined grain size [15], and a discontinuous or continuous oxide layer was formed on the surface of c-Cu and nc-Cu and their counterparts [12,14]. Furthermore, it has been shown (e.g., in [16–18]) that the nature of the copper oxides has an effect on both friction and wear. In [24] it was shown that a low sliding speed can induce a transferred layer leading to copper–copper contact and high CoF above 1.0, whereas, at higher speed less material transfer occurs leading to a lower CoF. In [25] it was confirmed that the transferred Cu increases the friction. In [20] it was noted that similar materials in counterfaces can lead to an increased adhesion and higher CoF.

Tribological properties of Cu-Al_2O_3 and c-Cu, produced by PECS (pulsed electric current sintering), have been studied in [5] using reciprocating ball-on-flat method against corundum operated at 5 N. No major difference was noticed in steady state friction between Cu-Al_2O_3 and c-Cu, the CoFs being around 0.5–0.6, which was affected by the tribolayer, surface oxidation, and subsurface microstructure in the contact area. However, wear depth for the composite was less than half of that of c-Cu. Wear and friction of Cu-5 vol% Al_2O_3 was studied in [22] using ball-on-disk method with steel balls and 1 N load. Values of CoFs about 0.55–0.60 and wear rate for micron-sized composite about 1×10^{-3} mm^3/Nm and for the nanocomposite about 3×10^{-4} mm^3/Nm were obtained. The study [23] showed CoF of about 0.73 and wear rate of about 1.4×10^{-3} mm^3/Nm for GlidCop® AL-60 (with 2.5 vol% Al_2O_3) at room temperature, whereas both values were lower at higher temperatures. Moreover, the same materials after ECAP (equal-channel angular pressing) showed refinement in grain size and lower CoF (0.64) and wear rate (1.2×10^{-3} mm^3/Nm).

Dry sliding wear properties of Cu-3 wt% diamond-0.5 wt% La composites and Cu were studied against bearing steel in [26]. The composite had lower CoF and wear rate than Cu, with respective CoFs of about 0.095 and 0.108 and wear rates of about 2×10^{-4} and 3.5×10^{-4} mm^3/Nm at a load of 50 N. The increased load led to lower CoFs, but higher wear rates. The main wear mechanisms of the composite were abrasive and adhesive wear, whereas for Cu those were oxidational wear, severe adhesive wear and fatigue. Much higher CoFs between 1.1 and 0.85 were reported in [21] for copper with clustered diamonds (CD) against tool steel. With increasing amount of CD's from 0 to 10 vol%, the CoF decreased but the wear rate increased. No tribological studies on Cu with isolated diamonds have been found. Similarly, the lubricating effect of copper oxides formed during the sliding tests has been investigated, whereas, no tribological studies were found for as-prepared bulk Cu-Cu_2O composite samples. On the contrary, e.g., TiB_2 [19,27], SiC [20], and graphite [28] have successfully been applied to enhance wear properties, and carbon nanotubes (CNTs) [29] and graphite [28] to reduce CoF as compared to plain Cu.

PECS has been applied for different materials [30]. Earlier we have employed PECS in preparing dense and fine-grained Cu-composites with improved mechanical properties and temperature stability as compared to Cu [31]. In the present work, the tribological properties of these composites are studied in sliding tests. Even if tribological issues have been studied for several Cu-composites, the focus usually has been on only one or two different types of the composites. In the present work, 16 different types of Cu-composites are compared at the same time in the same manner. As the main focus of the work is on the comparison of these different material combinations, two different types of counter materials, metallic and ceramic, were chosen to highlight the differences in wear rate and mechanisms involved in different types of mating surfaces under the same test conditions.

It is believed that the results of this study serve as a basis for the selection of materials for electric connector

parts. Furthermore, it exploits the potential of the PECS technique in preparing high-quality Cu-composite materials.

2. EXPERIMENTAL DETAILS

2.1. Materials

The materials studied were PECS Cu-composites made by FCT HP D 25 PECS equipment. The starting powders, as well as the process parameters for PECS are described in greater detail in our previous study [31]. Briefly, the sintering temperatures were from 773 to 1323 K, pressures from 50 to 100 MPa, and holding times up to 6 min depending on the type of the starting powder. With a few exceptions, the Cu-composites, chosen for tribological study, had a density above 97% of T.D. and all were harder than the plain copper (Table 1). The selection of the test materials consisted of Cu with: (i) semiconductive Cu_2O [3], (ii) stable but electrically non-conductive Al_2O_3 [5,31,32], (iii) thermally conductive nano- and submicron-sized diamonds (nanoD/ND/SMD) [26], or (iv) electrically conductive and thermally stable TiB_2 [19,31]. The materials along with the amount and type of dispersoids and microhardness values are presented in Table 1. The PECS compacted cylindrical samples were ground and polished using normal metallographic sample preparation procedure. The final polishing was accomplished by using colloidal silica slurry followed by ultrasonic cleaning in acetone and subsequently cleaning with ethanol before testing.

Table 1. Composition and microhardness of the PECS compacted samples

Sample designation	Sample description	Volume of dispersoids, %	Hardness, GPa
c-Cu	coarse-Cu	0	0.57
sm-Cu	submicron-Cu	0	1.08
20Cu_2O	sm-Cu with Cu_2O	20	1.23
37Cu_2O		37	1.34
12TiB_2	sm-Cu with TiB_2	12	1.78
20TiB_2		20	1.97
36TiB_2		36	2.47
79TiB_2		79	3.94
1.2Al_2O_3	c-Cu with Al_2O_3	1.2	1.22
2.5Al_2O_3		2.5	1.58
3ND	sm-Cu with 50 nm	3	1.46
6ND	diamonds	6	1.77
3SMD	sm-Cu with 250 nm	3	1.31
6SMD	diamonds	6	1.26
6nanoD	sm-Cu with 5 nm diamonds	6	2.02
nCu-6nanoD	nano-Cu with 5 nm diamonds	6	1.08

2.2. Sliding friction and wear test

The tribological properties were determined by dry reciprocating sliding ball-on-flat technique [6] using UMT-2 versatile nano-micro tribometer operated at 1 N normal force at room temperature (25 °C) in air with a relative humidity of about 45%. The ball-on-flat test method was chosen because the size of PECS samples (typically Ø 20 mm), provides enough sample surface for ball-on-flat sliding test, whereas the sample is not large enough for, e.g., the pin-on-disk test. The test conditions were chosen to represent the possible conditions in (separated) electrical connectors, with possible back-and-forth type of micromotions rather than one-directional gliding, low applied load, non-lubricated conditions, and non-shielded atmosphere. The load was determined based on the Hertz contact stress evaluation, so that in a static situation it would not cause plastic deformation in coarse copper. The diameter of the studied disc-shaped samples was either 20 or 25 mm with a thickness of 3 to 6 mm. The friction and wear tests were carried out at a displacement amplitude of 5000 μm with sliding frequency of 5 Hz up to 3000 cycles. Tests were run for 10 min resulting in a total distance of 30 m. Two different counterparts were used: 3 mm sized Cr-steel balls with 1.6% Cr (100Cr6) with hardness of 700 HV (6.86 GPa) and 3 mm sized alumina balls with hardness of 1700 HV (16.7 GPa). During the experiments, the coefficient of friction μ was recorded as a function of time and the values in the middle of each displacement amplitude were collected for reporting.

2.3. Sample characterization

After sliding tests, the width and surface of the wear tracks were studied with an optical microscope and scanning electron microscopy (SEM) (Hitachi FE-SEM S-4700 equipped with Inca EDS). The optical images were taken in order to study the widths of the wear tracks in different types of test materials, whereas SEM was applied for morphology and elemental studies for selected samples only. Also, the surfaces of counter balls were studied with the optical and scanning electron microscopy to observe in greater detail the wear mechanisms. Profiles of the worn surfaces were measured from flat surface, ignoring possible pile-ups, by a Dektak 6m stylus profilometer to determine the depth and shape of the wear track. The cross-section of each track was measured at three to five different locations along the track to calculate the average cross-sectional worn areas. The volume loss was then calculated based on the average cross-sectional worn area and longitude stroke length (5000 μm). The specific wear rates (W) were expressed according to ISO 20808 [33] as the volume loss (V) per distance (L) and applied load (F_p):

$$W = \frac{V}{LF_p},\ \text{mm}^3/\text{Nm}. \quad (1)$$

Few of the samples were prepared for cross-sectional and longitudinal sections to carry out subsurface microstructural observations of worn tracks by SEM. Also the microhardness values (0.2 HV) were measured on the worn tracks for each type of samples to evaluate if reciprocated sliding was inducing work-hardening at the worn surface.

3. RESULTS

3.1. Friction behaviour

Figure 1 presents few examples of CoF evolution during the sliding tests under a load of 1 N. In Fig. 1a, the CoFs were recorded during tests with Cr-steel counter balls, illustrating a notable fluctuation in tests, whereas those seen in Fig. 1b with alumina balls indicate a uniform sliding behaviour. In general, it takes slightly more time to reach the steady state values with the Cr-steel ball than with the alumina ball. Sliding against alumina balls is characterized with smoother sliding, lower CoFs, and quickly reached steady state. It seems that the CoF values against Cr-steel converge at the end of tests closer to CoF values of Cu, whereas the difference in CoF values against alumina remain large and relatively stable throughout the test. It is suggested that Cu matrix dominates in sliding against Cr-steel and the type or amount of dispersoids has smaller influence. On the contrary, the influence of the type of dispersoids is more notable when sliding against alumina. In both cases, the highest CoF values at the end of tests were for $79TiB_2$ samples and lowest for $37Cu_2O$ samples. Even if Fig. 1 presents only few examples, the results were similar within the same type of materials with good repeatability. Further proof of this is presented in Fig. 2, which combines all the test results (with standard deviations). The averaged CoFs were taken from steady state region (i.e. between 400 and 600 s) based on two/three experiments. The results show typically 0.2–0.4 higher CoFs against Cr-steel than against alumina. Whereas the CoFs decrease with increasing Cu_2O, on the contrary for Cu-Al_2O_3 and Cu-diamond the increasing amount increases the CoFs against Cr-steel. For Cu-TiB_2 the CoF is lowest for $12TiB_2$, however, for other samples it is near to the value of 1.0. Similar trends (Fig. 2) were attained in sliding against alumina, except for Cu with 5 nm sized diamonds (Cu-nanoD), which shows quite the same CoF than sm-Cu and for $1.2Al_2O_3$ which indicates low CoF.

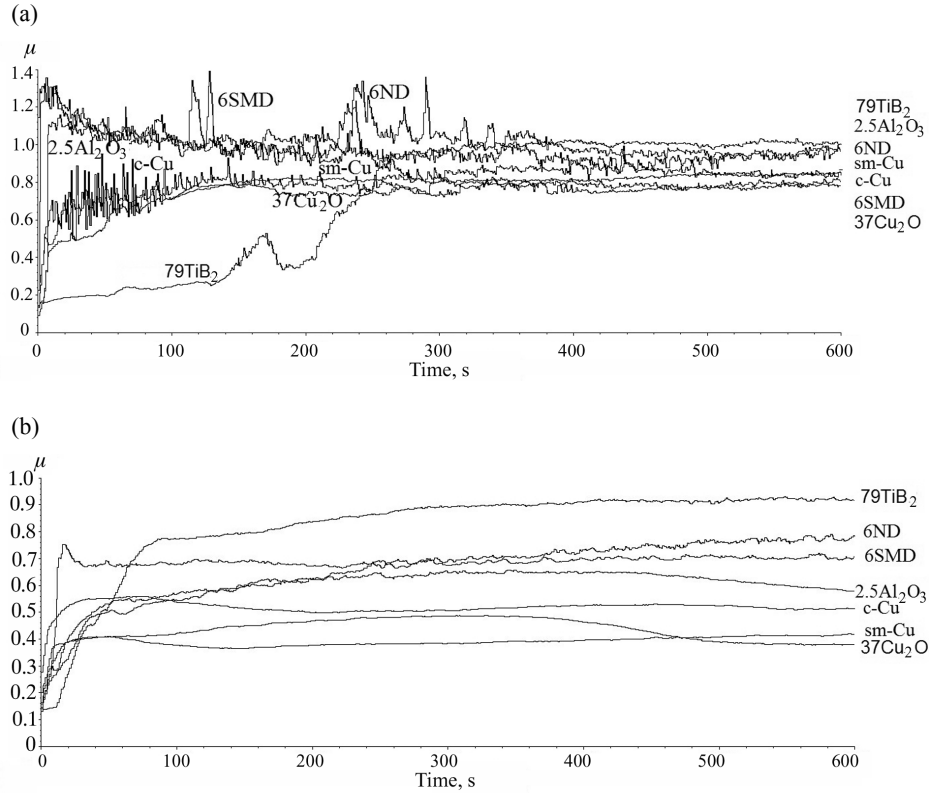

Fig. 1. Evolution of the coefficient of friction μ for selected composites with time against Cr-steel (a) and alumina counter (b) balls.

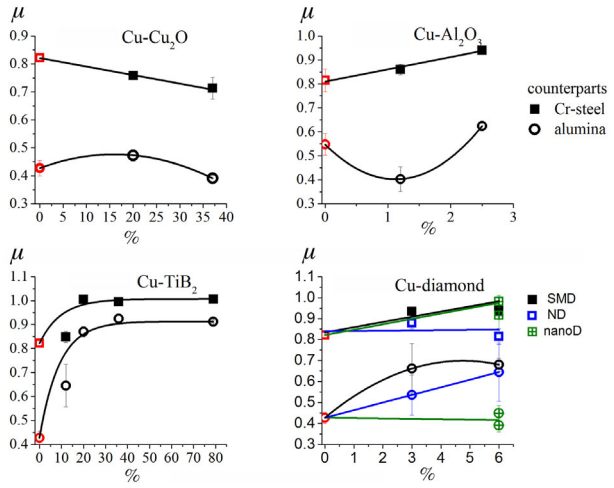

Fig. 2. The steady state coefficient of friction μ as a function of vol% of dispersoids for each type of Cu-composites against Cr-steel and alumina counter balls. Note that the scales are different. The red marks are reference values for Cu (c-Cu for Cu-Al_2O_3 composites, and sm-Cu for others).

3.2. Wear behaviour

Wear behaviour of each type of Cu-composites and Cu samples is quite different depending on the used counter material. Figure 3 shows the optical images of the wear tracks for each sample demonstrating large wear in tests against Cr-steel (upper images), and low wear in tests against alumina (lower images). It also indicates that Cu-Cu_2O (37Cu_2O) presents best performance against Cr-steel, whereas, for Cu-Al_2O_3 (2.5Al_2O_3) and Cu-diamond (6ND and 6SMD) the wear behaviour was poor. Altogether, all the test materials showed much better behaviour against alumina, 6ND sample performing best, whereas, c-Cu showed the most notable wear. The SEM–EDS analysis made after the wear test on each type of composite and Cu samples is presented in Fig. 4. The analysis shows that oxygen plays a significant role in sliding wear for sm-Cu and 37Cu_2O and 79TiB_2 samples. The rough estimation of oxygen content obtained by SEM–EDS analysis along the wear track is more than 10 wt%, which is much more than outside the tracks and clearly has increased during the tests. In comparison, for c-Cu, 2.5Al_2O_3 and 6ND samples the oxygen content in wear tracks is about 3 wt%. Figure 4 also shows that material transfer from the counter balls has taken place. The amount of Fe is most notable for 79TiB_2 sample, probably because of its high hardness. Figure 5 shows few examples of the SEM–EDS analysis made on wear tracks after sliding against alumina balls indicating increased oxygen content in wear tracks. Same observation was made for each type of composite and both Cu reference samples.

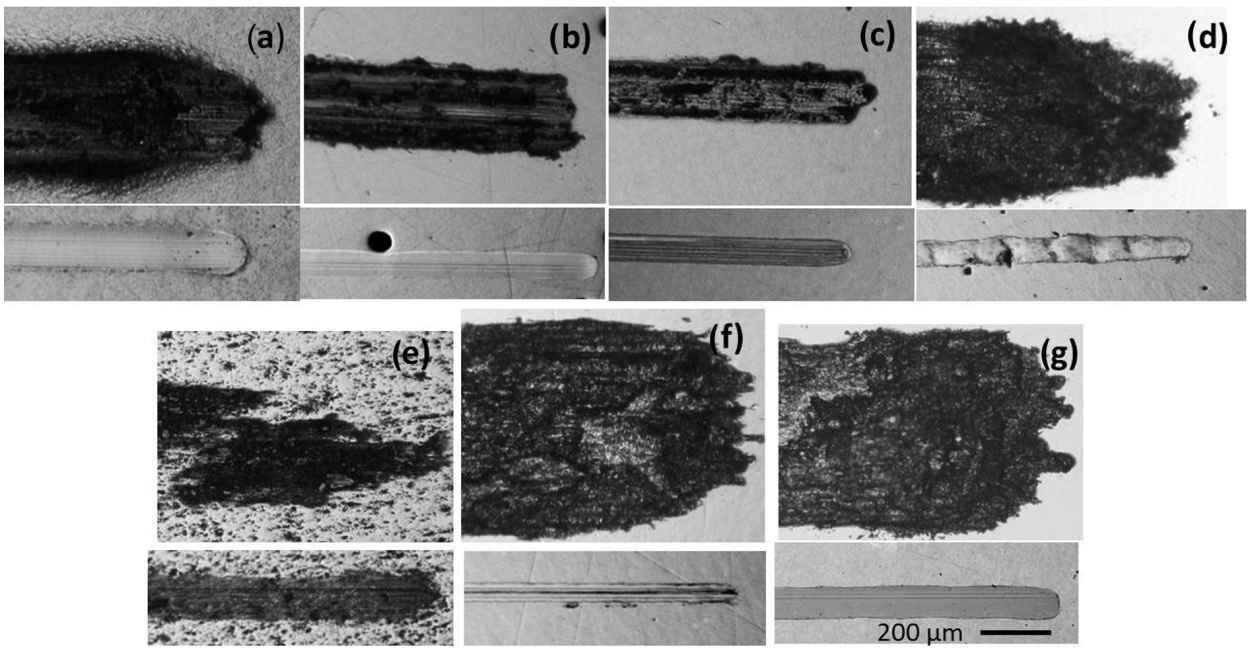

Fig. 3. Optical images of the wear tracks for (a) c-Cu, (b) sm-Cu, (c) 37Cu_2O, (d) 2.5Al_2O_3, (e) 79TiB_2, (f) 6ND, (g) 6SMD. The upper image in each picture shows the wear track made by the Cr-steel ball and the lower image that made by the alumina ball.

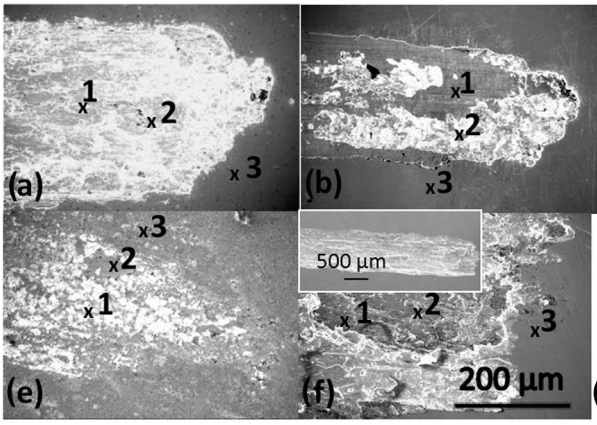

(g)

	point 1		point 2		point 3	
	O, %	Fe, %	O, %	Fe, %	O, %	Fe, %
a) c-Cu	2.8	1.4	3.0	1.5	0	0
b) sm-Cu	10.7	0.9	9.2	1.1	0	0
c) $37Cu_2O$	11.6	0.9	10.3	0.9	2.4	0
d) $2.5Al_2O_3$	2.8	0.8	2.9	0	1.2	0
e) $79TiB_2$	32.7	23.4	34.1	55.8	4.3	0
f) 6ND	3.0	2.5	1.6	0	0	0

Fig. 4. Morphologies of the worn surfaces made by Cr-steel balls: (a) c-Cu, (b) sm-Cu, (c) $37Cu_2O$, (d) $2.5Al_2O_3$, (e) $79TiB_2$, (f) 6ND; (g) SEM–EDS analysis of the points shown in (a)–(f) indicative of the amount of O and Fe (wt%).

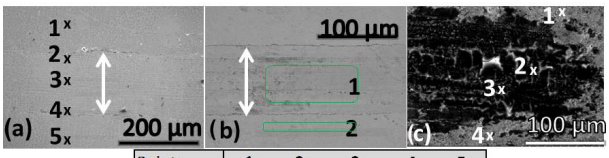

(d)

Point	1	2	3	4	5
	O, %				
a) c-Cu	0.0	1.0	7.0	2.5	0.0
b) $37Cu_2O$	5.1	1.5			
c) $79TiB_2$	0.0	30.8	47.5	0.0	

Fig. 5. Morphologies of the worn surfaces created by sliding alumina ball. (a) c-Cu, (b) $37Cu_2O$, (c) $79TiB_2$, (d) SEM–EDS analysis of the points shown in (a)–(c) indicating the rough amount of O (wt%). In (a) and (b) the width of the wear track is indicated by an arrow.

Microhardness values (0.2 HV) were measured on the wear tracks after sliding against Cr-steel to evaluate if worn surface has hardened due to the reciprocating sliding. The hardness measurements showed an increment from 8% to 76% as compared to the hardness values from outside the tracks. The $79TiB_2$ sample, being hardest, presented the lowest increment of 8%, while the samples sm-Cu, $37Cu_2O$, $2.5Al_2O_3$, 6ND, and $12TiB_2$ yielded in increments of between 15% and 33%, and c-copper, as the softest sample, showed 76% increment to the initial hardness value. Hardness measurements were not carried out for the small-sized tracks (between the widths of 30 and 150 µm) made by alumina balls.

After the sliding tests, all the Cr-steel counter balls were studied with optical microscope (Fig. 6) and the selected balls with SEM (Fig. 7). The abrasive and

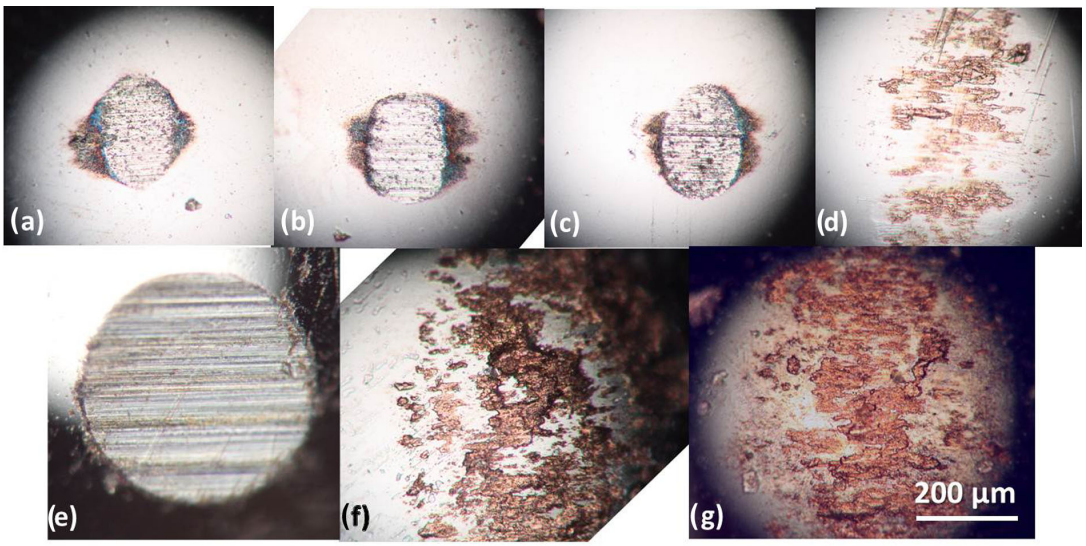

Fig. 6. Optical micrographs of the Cr-steel counter balls after wear tests against: (a) c-Cu, (b) sm-Cu, (c) $37Cu_2O$, (d) $2.5Al_2O_3$, (e) $79TiB_2$, (f) 6ND, (g) 6SMD. The scale is the same in all pictures and the sliding direction is horizontal.

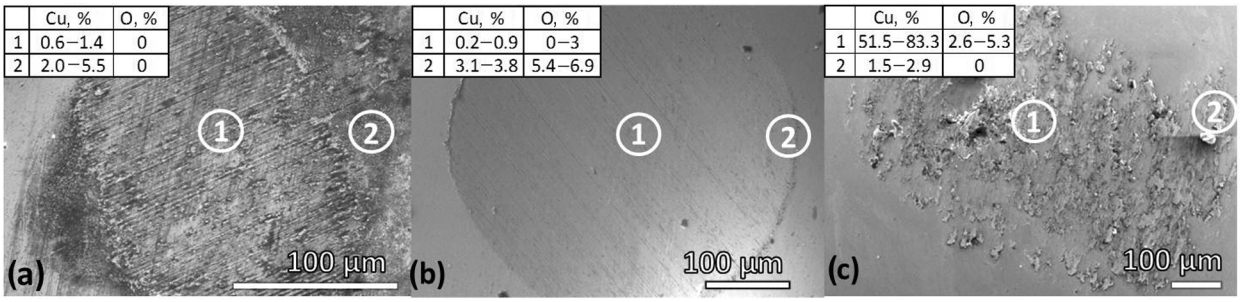

Fig. 7. SEM micrographs and SEM–EDS analysis of the Cr-steel counter balls after sliding against (a) c-Cu, (b) 79TiB_2, (c) 6ND. The SEM–EDS analysis was made from areas inside and at the edge of the sliding surfaces of the ball to show the amounts of transferred Cu and O in oxides.

Table 2. Tribological properties (CoF, wear rate and main wear mechanism) of the test samples in contact with Cr-steel and alumina counter balls. Reference values from literature are included for CoF and wear rates

Sample	CoF		Wear rate, mm^3/Nm		Main wear mechanisms*		Reference values for COF/wear rate (counter material)	References
	Cr-steel	Alumina	Cr-steel	Alumina	Cr-steel	Al_2O_3		
c-Cu	0.81	0.55	2.0E-04	6.1E-06	ABR (+ OX)	OX (pile-ups)	0.6 (Al_2O_3) 0.74 (WC-Co) 0.5–1.1 (steel) 3.5E-04 (steel) 4E-05 (Al_2O_3)	[5,6,12,21, 24,26,34]
sm-Cu	0.82	0.43	2.6E-05	4.0E-06	ABR + OX	OX	nCu 0.54 (WC-Co)	[12]
20Cu_2O	0.76	0.47	2.9E-05	1.9E-06	ABR + OX	OX	No reference values found	
37Cu_2O	0.71	0.39	1.3E-05	1.0E-06	ABR + OX	OX		
20TiB_2	1.00	0.87	3.4E-05	5.7E-06	ABR + OX	OX	values for pure-TiB_2:	[6,35–37]
36TiB_2	1.00	0.92	2.1E-05	3.7E-06	ABR + OX	OX	0.5–0.9 (steel)	
79TiB_2	1.01	0.91	1.5E-05	2.8E-06	ABR + OX	OX + ABR	0.5–0.7 (Al_2O_3)	
12TiB_2	0.85	0.65	2.1E-03	1.3E-06	ADH	OX (pile-ups)	8E-05–1.9E-04 (steel) 1E-06 (Al_2O_3)	
1.2Al_2O_3	0.86	0.40	4.7E-04	2.4E-07	ADH	OX (pile-ups)	0.55–0.73 (steel)	[5,22,23]
2.5Al_2O_3	0.94	0.62	5.0E-04	2.8E-06	ADH	OX	0.5–0.6 (corundum) 3E-04–1.4E-03 (steel)	
3ND	0.93	0.54	2.4E-03	7.3E-07	ADH	OX	0.095–1.1 (steel)	[21,26]
6ND	0.94	0.64	2.6E-03	2.4E-07	ADH	OX	2E-04 (steel)	
3SMD	0.88	0.66	1.1E-03	8.9E-07	ADH	OX		
6SMD	0.81	0.68	2.3E-03	1.5E-06	ADH	OX		
6nanoD	0.98	0.45	5.7E-03	1.4E-07	ADH	OX		
nCu-6nanoD	0.92	0.40	3.9E-04	7.8E-07	ABR + ADH	OX (pile-ups)		

* ABR – abrasive, ADH – adhesive, OX – oxidational.

adhesive wear mechanisms were identified based on the ball surfaces. Examples in Fig. 6 indicate that abrasive wear and some wear debris (in circumference) have taken place for c-Cu, sm-Cu, and 37Cu_2O, whereas sample 79TiB_2 caused large wear on the ball surface (Fig. 6a–c and e). On the other hand, adhesive wear was confirmed for 2.5Al_2O_3, 6ND, and 6SMD samples after sliding against Cr-steel. The balls were more or less covered by Cu from the samples (Fig. 6d, f, and g). Examples of SEM–EDS analysis taken from ball surfaces in Fig. 7 for c-Cu, 79TiB_2, and 6ND verify the observations made on Fig. 6. Some material transfer from test samples can be observed, especially in the test with 6ND; the ball was covered by Cu over a large area with pile-ups also. The imaging and analysis of alumina balls showed no adhesive wear and only the hardest sample, 79TiB_2, caused slight abrasive wear on the ball surface and some material transfer from alumina ball to wear track. The observed wear mechanisms are summarized in Table 2.

3.3. Wear profiles and wear rate

Figure 8a shows the typical cross-sectional profiles of the wear tracks created on each type of samples by the Cr-steel ball. It can be seen that the depth of wear tracks in $2.5Al_2O_3$, $12TiB_2$, and 6ND is much greater than for c-Cu, whereas the depths are clearly less for sm-Cu, $37Cu_2O$, and $79TiB_2$. This figure confirms a notable pile-up for c-Cu, smooth wear profile for $37Cu_2O$, slightly rougher profile for sm-Cu, and wider as well as roughened but not so deep wear profile for $79TiB_2$. The wear profiles of the samples after sliding against alumina balls are much smoother, indicating less wear (Fig. 8b). Pile-ups were observed in case of c-Cu, $1.2Al_2O_3$, $12TiB_2$, and nCu-6nanoD samples. Pile-ups may lead to reduction of contact stresses and consequently lower wear rates. Figure 9a illustrates the longwise profile and Fig. 9b corresponding cross profile of the wear track of c-Cu. These figures indicate formation of the deformation layer during the reciprocated sliding. Figures 9c–e present the cross-section profiles of the wear tracks for sm-Cu, $37Cu_2O$, and 6SMD, respectively. The arrows in Fig. 9 indicate the surface of the wear track (cross-section profiles).

Characteristics of each of the studied sample are shown in Table 2. Information includes the measured CoFs, wear rate, wear mechanisms, and some reference values found in the literature. The wear rates and plots in Fig. 10 (logarithmic scale) verify higher wear rates of samples after sliding against Cr-steel as compared to those against alumina. The increased amount of Cu_2O decreases the wear rate against Cr-steel, whereas, an addition of Al_2O_3 or diamond increase the wear rate as compared to pure sm-Cu. The sample $12TiB_2$ presented high wear rate against Cr-steel, although, a decreasing wear rate can be noticed as the content of TiB_2 increased. General trend shows that greater amount of dispersoids decreases the wear rates against alumina as compared to the corresponding bare Cu samples. The two exceptions are $1.2Al_2O_3$ and $12TiB_2$, which both yielded in low wear rate with notable pile-up in sliding against alumina.

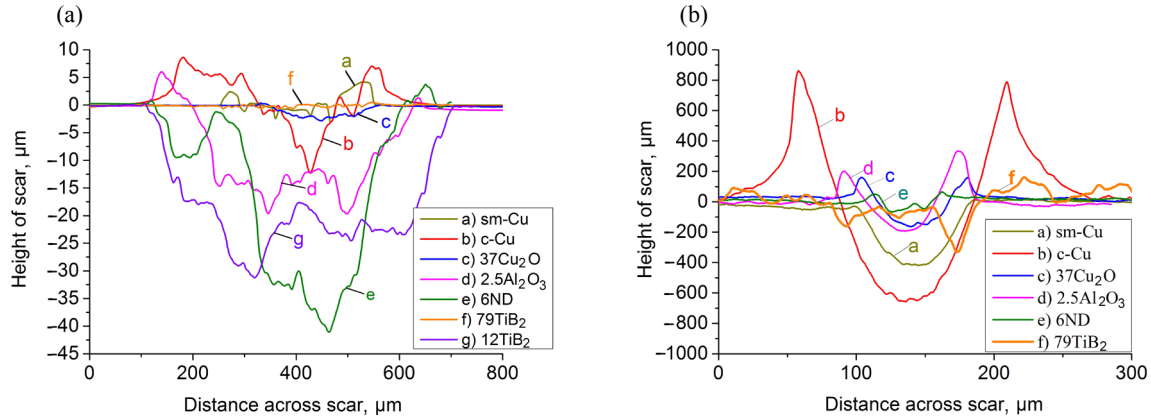

Fig. 8. Typical wear profiles of the tracks: (a) the Cr-steel counter ball, (b) the alumina counter ball.

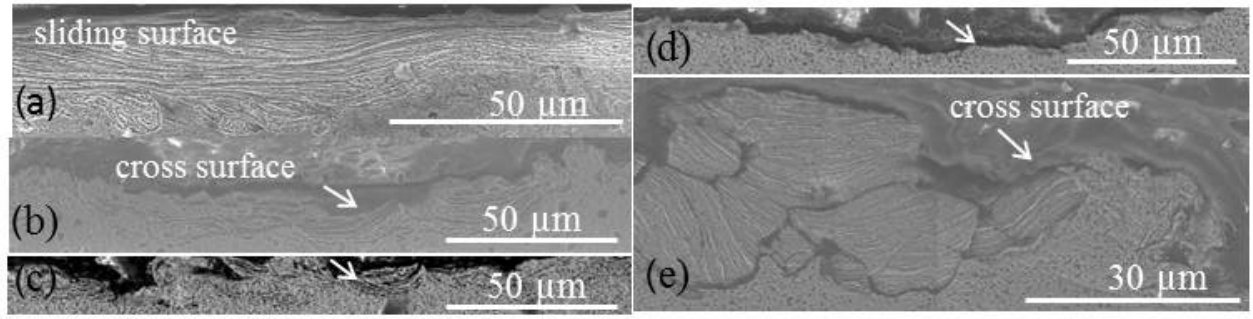

Fig. 9. Wear profiles taken with SEM from the wear tracks: (a) c-Cu in longitudinal direction, (b) corresponding cross-section profile and cross-section profiles for (c) sm-Cu, (d) $37Cu_2O$, and (e) 6SMD. Counter ball was Cr-steel.

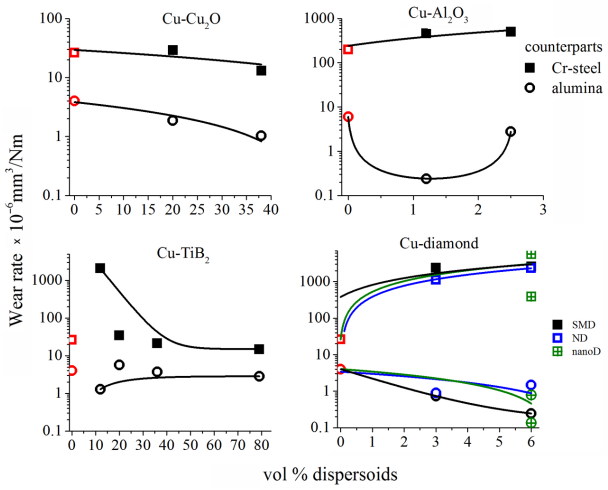

Fig. 10. The logarithmic presentation of the wear rates as a function of vol% dispersoids for each type of composites against Cr-steel and alumina. The reference Cu values (i.e. 0 vol% dispersoids) are marked as red (values of c-Cu for Cu-Al_2O_3 composites due to coarse matrix and sm-Cu for others).

4. DISCUSSION

The friction properties and wear rate of materials under different operating conditions are influenced by the composite composition, metallurgical structure, including interfaces [3,6], and properties of constituents (e.g. hardness/strength, grain size, wear resistance, ability for work-hardening or formation of transfer layer, thermal conductivity, and load bearing ability [5,12–15,20, 22,27,37]). Direct correlation of these and materials performance in tribological contact is challenging due to changes in material and its surface properties during sliding process and running-in period [3].

4.1. Coefficient of friction

Figure 1 confirms that the steady state is reached earlier in tests against alumina, whereas notable fluctuation occurs during the sliding against Cr-steel balls, leading to longer running-in periods. On the other hand, the steady state CoFs are clearly closer to each other in tests against Cr-steel as compared to those against alumina. The CoF fluctuation as well as its higher values are suggested to result from several reasons. Firstly, the combination of sliding materials that have higher reactivity against each other tends to have higher CoF and wear rate [3]. Metal–metal contact is thus much more reactive than metal–ceramic interface. Secondly, decohesion, material transfer, and adhering between the counterparts can have as the consequence destructive or unstable behaviour [18,38]. Thirdly, the frictional heating during sliding in air environment can cause oxidation of the Cu surface (appearing mainly in Cu_2O [3]), and the forming and destruction of the film can occur repetitively influencing the friction behaviour [5,14]. Moreover, it is possible that the fluctuation may be due to the pull-off of the hardened layer [14,38], especially, this could be the reason of high fluctuation for c-Cu during the running-in period (Fig. 1a). For Cu-diamond composites the fluctuation is also observable.

The steady state CoFs, presented in Fig. 2, indicate that Cu_2O in Cu matrix decreases the CoF values against both Cr-steel and alumina. Most types of dispersoids led to higher CoFs as compared to reference Cu samples (c-Cu and sm-Cu), which both yielded CoFs of about 0.8 against Cr-steel (Table 2) and CoF of 0.55 for c-Cu and 0.42 for sm-Cu against alumina. It has been reported that the fine-sized Cu leads to lower CoF [13,14]. One reason for that may be that the oxidation rate depends on the grain size, i.e., fine grains with higher boundary area are more easily oxidized, thus providing more lubricative contact [12,13]. Addition of 5 nm sized diamonds in Cu matrix seemed to decrease slightly the CoFs against alumina (CoF of 0.4, Table 2), whereas, the larger size and higher amount of diamonds led to higher CoFs as compared to sm-Cu (Fig. 2). Lubricating effect of diamonds has been reported to depend, e.g., on surface properties, carbon bonding on surface, size of diamonds, atmosphere and its humidity, and pH [39–41]. In [39] it was suggested that approximately 100 nm is the threshold size for the diamonds, the smaller being good solid lubricants in vacuum conditions. It was shown that the smaller-sized are the diamonds, the lower is CoF [39]. In general, the friction values in this study are slightly higher against steel than those reported elsewhere, while the measured CoFs against alumina are somewhat smaller than previously reported (Table 2).

4.2. Wear track profiles

The wear behaviour depend greatly on the counter material. The wear tracks were deep and wide after sliding against Cr-steel, especially for Cu-Al_2O_3 and Cu-diamond (Figs 3d, f, g, and 8a). When comparing the tracks induced by Cr-steel to those induced by alumina (Fig. 3), the 37Cu_2O sample showed about twice wider track, whereas the tracks for sm-Cu, 2.5Al_2O_3, and 6ND were about 2.5, 7, and 10 times wider, respectively. Moreover, when the wear depths (induced by Cr-steel) are compared to each other (Fig. 8), 37Cu_2O and sm-Cu showed depths of about 2 μm, whereas for samples 2.5Al_2O_3 and 6ND, the depths were about 10 and 20 times bigger (i.e. 20 and 40 μm), respectively. Against alumina, the wear tracks were smooth and from 30 to 150 μm wide for all the tested materials, whereas the depths were between 50 and 350 nm for Cu-composites, about 400 nm for sm-Cu, and about 700 nm for c-Cu with quite extensive pile-ups (Figs 3 and 8b). When the contact pressure exceeds the yield strength, the material

flows into the sides of the wear track and the surface along the wear track is work hardened [5,6,12]. Since c-Cu has low hardness (Table 1), the reciprocating sliding can cause more material pile-ups to the sides of tracks and repetitive work-hardening in the worn surface [5,12,13,18]. In paper [12] it was proposed that plastic deformation occurs to a lesser extent in hard nc-Cu than soft large-grained Cu, because of its higher hardness resulting in less work-hardening of subsurface. We observed over 70% increase in the hardness of c-Cu after reciprocating sliding against Cr-steel. The effect of sliding on the worn substructure (Fig. 9) revealed that the deformation layer of c-Cu extended deeper than that of sm-Cu or 37Cu_2O, the thickness of the deformed layers being 20–25 μm, 5–10 μm, and a few μm, respectively. The appearance of the wear tracks was also quite different for these samples. The surface for c-Cu and sm-Cu were quite rough, while that of 37Cu_2O was smooth (see Fig. 9). The subsurface of 6SMD indicate deformed and large areas of spalling-off material partly covering the worn surface. This indicates that some of the surface material has been deformed and fractured due to the cyclical stresses, and then moved to another place during sliding. This can be partly relating to the significant fluctuation of CoF during the sliding tests (Fig. 1). The use of Cr-steel balls against Cu-diamond samples led to extensive wear tracks, whereas, against alumina those performed much better yielding in smaller tracks with decreasing size of dispersoids. It has been widely recognized that carbon in diamond can diffuse into steel at higher temperatures, and thus diamond is not suitable, e.g., for tooling of ferrous alloys [3,6,40–42]. E.g., in [42] it is reported that comparable wear on the diamond tool from steel with similar hardness was encountered at cutting distances 1000 times less than for the aluminum. Moreover, it has been pointed out that water absorption from air can make surface more sensitive to adhering, and surface state of diamonds can also effect adhesion sensitivity in sliding [37,40,41,43]. In general, the profiles of the wear tracks made by Cr-steel balls led to much wider and deeper worn areas than alumina ball.

4.3. Wear rate and mechanism against Cr-steel counter ball

The main reason for extensive wear of samples in tests against Cr-steel is the wear mechanism involved. The transfer of material from one surface to another is the prime symptom of adhesion [3], and careful analysing of the Cr-steel counter ball surfaces after sliding revealed severe adhesive wear of Cu-diamond and Cu-Al_2O_3 (see Figs 6d, f, g, and 7c), and correspondingly very high wear rate (Table 2 and Fig. 10). The same composites showed also very high friction of about 1.3 already after 5 s of the experiments (Fig. 1a). Sample 12TiB_2 showed also adhesive wear, deep wear track, high wear rate (Figs 8a, 10 and Table 2), and also high initial friction (1.15) in the beginning of the experiment.

Figure 3 shows the worn surfaces after sliding against Cr-steel. For c-Cu, 2.5Al_2O_3, and 6ND the wear tracks have rough surface with some oxygen (Fig. 4), whereas the smoother surfaces with higher oxygen content can be observed for sm-Cu, 37Cu_2O, and 79TiB_2. It is suggested that non-uniform oxidational wear (forming and destruction of oxide film) plays a role in sliding, especially for samples with higher amount of oxygen. For samples with adhesive wear, the adherent behaviour started already in the very beginning of the tests, thus leading to high wear rates. The samples, which revealed abrasive wear and/or oxidational wear in sliding contact, based on the analysis of counter surfaces, resulted in much lower wear rate and initially also lower CoFs. Abrasive wear was identified in the case of Cr-steel balls sliding against c-Cu, sm-Cu, Cu-Cu_2O, and Cu-TiB_2 (>20 vol%). The counterpart surfaces showed many parallel and uniform furrows typical for abrasive wear [3]. Further proof was obtained as abrasive particles and wear debris was found at the end of furrows. Those were observed primarily at the entrance/exit points of the balls (e.g. Figs 6a–c and 7a), whereas Fe transferred from counter balls was present at the 'end-points' of wear tracks (Fig. 4). Detached wear debris particles are removed from surface and have abrasive effect when rubbing in contact area [18]. For TiB_2 (>20 vol%) and Cu_2O containing composites, the wear rate tends to decrease as the amount of dispersoids increase, whereas, an addition of Al_2O_3 or diamond increases the wear rate. Thus Cu composites with diamond or Al_2O_3 dispersoids are not suitable for contact with steel. The studied materials showed high wear rates between 1.3×10^{-5} and 5.7×10^{-3} mm^3/Nm against Cr-steel (Table 2).

4.4. Wear rate and mechanism against Al_2O_3 counter ball

Oxidational wear was identified in SEM and SEM–EDS analysis on the worn surfaces of all the tested samples (Figs 3 and 5) after sliding against alumina counter balls. The worn surfaces showed smooth profile (Fig. 8b) and non-destructed sliding surfaces (Fig. 3) with increased oxygen content (Fig. 5) and these features were observed for each type of the samples. Low wear rates are caused by non-reactive contact parts with lubricative surface oxidation induced by the environmental and frictional conditions. Some of the samples showed notable pile-up, thus part of the sliding tracks were associated with extensive material transfer from the sliding surface to the two sides. For Cu_2O and TiB_2 (>20 vol%) and diamond composites the wear rate showed decreasing trend as the amount of dispersoids increased. The sample with lower amount of Al_2O_3 in Cu leads to lower

wear rate against alumina than with higher amount. This might be due to slight changes in the wear mechanism, as has been pointed out in [44], where it is shown that more than 2 wt% Al_2O_3 leads to increased wear rate due to the change in the wear mechanism. With 1 wt% Al_2O_3 the mechanism was adhesive wear associated with oxidational wear, whereas, for higher amount of 2 wt% Al_2O_3 slight abrasive wear was noticed, and even higher amount (5 wt% Al_2O_3) led to abrasive wear, associated with delaminating fatigue [44]. Overall, the oxidational wear led to quite low wear rates between 1.4×10^{-7} and 6.1×10^{-6} mm^3/Nm (Table 2). The lowest wear was measured for Cu-diamond composites.

4.5. Notes on wear characteristics

From Fig. 10 it can be observed that the wear rate is less for fine-sized Cu (sm-Cu) than for coarse Cu (c-Cu) against both the counter materials. This is an obvious result of higher hardness of the sm-Cu compared to c-Cu. Similar hardness dependence of copper wear rate has been reported earlier [12,13,15]. The observations showed that the highest wear rates are caused by adhesive wear between the contact materials, whereas oxidational and abrasive wear led to lower wear on the samples. The comparison of the wear rate values with those from literature is somewhat challenging due to the different forms of reporting (worn area/volume/mass/intensity etc.), variation in counter materials, test conditions, etc. Some reference values for CoF and wear rate are shown in Table 2. When comparing the wear performance of different composites in this study, it seems that adhesively worn samples against Cr-steel showed highest wear rates and the CoFs at the end part of the test were mainly influenced by the copper matrix and did not depend so much on the type or amount of dispersed particles than in the beginning of wear. This led to friction values approach to those reported for copper-steel sliding pair. On the other hand, due to oxidational wear the lower wear rates were achieved when the same samples were tested against ceramic alumina counter ball. Also CoFs in these tests varied more, depending on the type and amount of dispersoids as well as on the wear mechanism, but were more stable troughout the test than against Cr-steel ball.

Usually the deterioration in the wear resistance has been attributed to an increase in reinforcement breakage, reinforcement pull out, and poor reinforcement-matrix interfacial bonding [19,20]. When the interfacial bonding is good, the wear resistance increases, e.g. due to the enhanced load-bearing ability as the amount of dispersoids increases [19,20,27]. Our earlier studies [31,45] have shown that a well-bonded interface between the diamonds and copper matrix is achieved by PECS. Thus, it is suggested that the high wear rates of Cu-diamond composites against Cr-steel are not because of the non-bonded interfaces but are more likely due to the interaction of diamonds with iron. It is noted that the diamond containing samples performed well against ceramic alumina balls showing mainly oxidative wear well below the level of plain copper.

5. CONCLUSIONS

In this work, the tribological properties of several Cu-composites prepared by PECS were studied against Cr-steel and alumina. The ball-on-flat test results showed great dependence for coefficient of friction (CoF), wear rate and wear mechanism on the used counterpart material. CoF was highest for Cu-TiB_2 (1.01) and lowest for Cu-Cu_2O (0.71). Reference coppers had a value 0.81–0.82. Cr-steel counter material showed reactivity against the metallic test samples leading to mainly adhesive wear and high wear rates between 1.3×10^{-5} and 5.7×10^{-3} mm^3/Nm. The Cu-Al_2O_3 and Cu-diamond composites showed much higher wear rates (adhesive wear) than other composites or the reference Cu. The highest wear rate was measured for Cu-diamond composites and the lowest for Cu-Cu_2O composite. It is believed that diamonds in the Cu-diamond composite reacted with iron in the counter material leading to accelerated wear in the composite. Materials, which showed abrasive or oxidational wear mechanisms, i.e. c-Cu, sm-Cu, Cu-Cu_2O, and Cu-TiB_2, had a lower wear rate.

Alumina counter material showed no reactivity against the test materials and led to lower CoFs from 0.39 (Cu-Cu_2O) to 0.92 (Cu-TiB_2), while the reference coppers had CoF of 0.43 (sm-Cu) or 0.55 (c-Cu). The main mechanisms acting on test materials were oxidational wear and pile-up formation, consequently leading to low wear rates between 1.4×10^{-7} and 6.1×10^{-6} mm^3/Nm. The lowest wear rate was measured for Cu-diamond composites, in the order of 5, 50, and 250 nm diamond dispersoids. All the composites were found to perform better than the plain reference Cu against alumina.

ACKNOWLEDGEMENTS

This work was supported by the Graduate School on Advanced Materials and Processes of the Academy of Finland. Estonian Science Foundation (personal grant ETF 8850 for Maksim Antonov) is also acknowledged.

REFERENCES

1. Groza, J. R. Heat-resistant dispersion-strengthened copper alloys. *J. Mater. Eng. Perf.*, 1992, **1**, 113–121.

2. Powder Metallurgy: Copper and Copper Alloys. *ASM Specialty Handbook*, ASM International, 2001, 105–120.
3. Peterson, M. B. A. and Winer, W. O. *Wear Control Handbook*. ASME, 1980, p. 1358.
4. Kumar, A. and Singh, S. *Wear Property of Metal Matrix Composite*. National Institute of Technology, Rourkela, 2011.
5. Eddine, W. Z., Matteazzi, P., and Celis, J.-P. Mechanical and tribological behavior of nanostructured copper-alumina cermets obtained by Pulsed Electric Current Sintering, *Wear*, 2013, **297**, 762–773.
6. Holmberg, K. and Matthews, A. *Coatings Tribology; Properties, Mechanisms, Techniques and Applications in Surface Engineering* (Briscoe, B., ed.). Tribology and Interface Engineering, Series 56, 2nd ed., 2009, p. 560.
7. Caron, R. N. Copper: Alloying. In *Encyclopedia of Materials: Science and Technology*. Elsevier, 2nd ed., 2001, 1652–1660.
8. Murty, Y. V. Electrical and electronic connectors: materials and technology. In *Encyclopedia of Materials: Science and Technology*. Elsevier, 2nd ed., 2001, 2483–2494.
9. Kaczmar, J. W., Pietrzak, K., and Włosiński, W. The production and application of metal matrix composite materials. *J. Mater. Process. Technol.*, 2000, **106**, 58–67.
10. Nadkarni, A. V. and Klar, E. Dispersion strengthening of metals by internal oxidation, SCM Corporation, 1973. U.S. Patent 3,779,714.
11. Sullivan, J. L. Oxidational wear of the metals. www.irg-woem.org/pdfs/15_6.pdf (accessed 14.06.2013).
12. Han, Z., Lu, L., and Lu, K. Dry sliding tribological behavior of nanocrystalline and conventional polycrystalline copper. *Tribol. Lett.*, 2006, **21**, 47–52.
13. Zhang, Y. S., Han, Z., Wang, K., and Lu, K. Friction and wear behaviors of nanocrystalline surface layer of pure copper. *Wear*, 2006, **260**, 942–948.
14. Zhang, Y. S., Han, Z., and Lu, K. Fretting wear behavior of nanocrystalline surface layer of copper under dry condition. *Wear*, 2008, **265**, 396–401.
15. Yao, B., Han, Z., Li, Y. S., Tao, N. R., and Lu, K. Dry sliding tribological properties of nanostructured copper subjected to dynamic plastic deformation. *Wear*, 2011, **271**, 1609–1616.
16. Senouci, A., Zaidi, H., Frene, J., Bouchoucha, A., and Paulmier, D. Damage of surfaces in sliding electrical contact copper/steel. *Appl. Surf. Sci.*, 1999, **144–145**, 287–291.
17. Liang, H., Martin, J.-M., and Lee, R. Influence of oxides on friction during Cu CMP. *J. Electronic Mater.*, 2001, **30**, 391–395.
18. Bouchoucha, A., Chekroud, S., and Paulmier, D. Influence of the electrical sliding speed on friction and wear processes in an electrical contact copper-stainless steel. *Appl. Surf. Sci.*, 2004, **223**, 330–342.
19. Yum, Y. J., Lee, K. S., Kim, J. S., Kwon, Y. S., Chang, M. G., Kwon, D. H., and Sung, C. H. Mechanical properties of Cu-TiB_2 nanocomposite by MA/SPS. In *Proc. 9th Russian–Korean International Symposium on Science and Technology KORUS, 2005*.
20. Zhan, Y., Zhang, G., and Zhuang, Y. Wear transitions in particulate reinforced copper matrix composites. *Mater. Trans.*, 2004, **45**, 2332–2338.
21. Sano, T., Murakoshi, Y., Takagi, H., Homma, T., Takeishi, H., and Mayuzumi, M. Characterization of diamond-dispersed Cu-matrix composites. *Mater. Trans.*, 1996, **37**, 1132–1137.
22. Hvizdoš, P. and Besterci, M. Effect of microstructure of Cu-Al_2O_3 composite on nano-hardness and wear parameters. *Chem. Listy*, 2011, **105**, 696–699.
23. Hvizdoš, P., Kulu, P., and Besterci, M. Tribological parameters of copper-alumina composite. *Key Eng. Mater.*, 2012, **527**, 191–196.
24. Emge, A., Karthikeyan, S., Kim, H. J., and Rigney, D. A. The effect of sliding velocity on the tribological behavior of copper. *Wear*, 2007, **263**, 614–618.
25. Sulek, W. and Jedynak, R. The effect of electroplated copper and zink coatings on friction conditions. *Mater. Sci.*, 2003, **9**, 258–261.
26. Zheng, R. G., Zhang, Z., Peng, X. T., and Wang, W. K. Dry sliding wear behavior of sintered copper-diamond composite fabricated by powder metallurgy. *Adv. Mater. Res.*, 2010, **139–141**, 335–339.
27. Tu, J. P., Rong, W., Guo, S. Y., and Yang, Y. Z. Dry sliding wear behavior of in situ Cu-TiB_2 nanocomposites against medium carbon steel. *Wear*, 2003, **255**, 832–835.
28. Moustafa, S. F., El-Badry, S. A., Sanad, A. M., and Kieback, B. Friction and wear of copper-graphite composites made with Cu-coated and uncoated graphite powders. *Wear*, 2002, **253**, 699–710.
29. Trinh, P. V., Trung, T. B., Thang, N. B., Thang, B. H., Tinh, T. X., Quang, L. D., Phuong, D. D., and Minh, P. N. Calculation of the friction coefficient of Cu matrix composite reinforced by carbon nanotubes. *Comp. Mater. Sci.*, 2010, **49**, 239–241.
30. Orrù, R., Licheri, R., Locci, A. M., Cincotti, A., and Cao, G. Consolidation/synthesis of materials by electric current activated/assisted sintering. *Mat. Sci. Eng. R*, 2009, **63**, 127–287.
31. Ritasalo, R., Kanerva, U., and Hannula, S.-P. Thermal stability of PECS-compacted Cu-composites. *Key Eng. Mater.*, 2013, **527**, 113–118.
32. Fathy, A., Shehata, F., Abdelhameed, M., and Elmahdy, M. Compressive and wear resistance of nanometric alumina reinforced copper matrix composites. *Mater. Design*, 2012, **36**, 100–107.
33. ISO 20808:2004(E). Fine ceramics – Determination of friction and wear characteristics of monolithic ceramics by ball-on-disk method. 2004.
34. Winzer, J., Weiler, L., Pouquet, J., and Rödel, J. Wear behavior of interpenetrating alumina-copper composites. *Wear*, 2011, **271**, 2845–2851.
35. Sánchez-López, J. C., Abad, M. D., Justo, A., Gago, R., Endrino, J. L., Garcia-Luis, A., and Brizuela, M. Phase composition and tribomechanical properties of Ti-B-C nanocomposite coatings prepared by magnetron sputtering. *J. Phys. D: Appl. Phys.*, 2012, **45**, 375–401.
36. Murthy, T. S. R. Ch., Basu, B., Srivastava, A., Balasubramaniam, R., and Suri, A. K. Tribological properties of TiB_2 and TiB_2-$MoSi_2$ ceramic composites. *J. Eur. Ceram. Soc.*, 2006, **26**, 1293–1300.

37. Wäsche, R., Klaffke, D., and Troczynski, T. Tribological performance of SiC and TiB_2 against SiC and Al_2O_3 at low sliding speeds. *Wear*, 2004, **256**, 695–704.
38. Luo, S. Y., Kuo, J. K., Tsai, T. J., and Dai, C. W. A study of the wear behavior of diamond like carbon films under the dry reciprocating sliding contact. *Wear*, 2001, **249**, 800–807.
39. Gubarevich, A. V., Usuba, S., Kakudate, Y., Tanaka, A., and Odawara, O. Frictional properties of diamond and fullerene nanoparticles sprayed by a high-velocity argon gas on stainless steel substrate. *Diamond Rel. Mater.*, 2005, **14**, 1549–1555.
40. Hollman, P., Wänstrand, O., and Hogmark, S. Friction properties of smooth nanocrystalline diamond coatings. *Diamond Rel. Mater.*, 1998, **7**, 1471–1477.
41. Paul, E., Evans, C. J., Mangamelli, A., McGlauflin, M. L., and Polvani, R. S. Chemical aspects of tool wear in single point diamond turning. *Prec. Eng.*, 1996, **18**, 4–19.
42. Lane, B. M., Shi, M., Dow, T. A., and Scattergood, R. Diamond tool wear when machining Al6061 and 1215 steel. *Wear*, 2010, **268**, 1434–1441.
43. Panda, K., Kumar, N., Sankaran, K. J., Panigrahi, B. K., Dash, S., Chen, H.-C., Lin, I.-N., Tai, N.-H., and Tyagi, A. K. Tribological properties of ultrananocrystalline diamond and diamond nanorod films. *Surf. Coat. Tech.*, 2012, **207**, 535–545.
44. Zhou, G., Ding, H., Zhang, Y., Hui, D., and Liu, A. Fretting behavior of nano-Al_2O_3 reinforced copper-matrix composites prepared by coprecipitation. *Metallurgija*, 2009, **15**, 169–179.
45. Ritasalo, R., Kanerva, U., Ge, Y., and Hannula, S.-P. Mechanical and thermal properties of pulsed electric current sintered (PECS) Cu-diamond compacts. *Metall. Mater. Trans. B*, 2013, 1–8, Published on-line.

Plasma-aktiveeritud paagutamisega valmistatud vaskkomposiitide kulumis- ja hõõrdekäitumise võrdlus

Riina Ritasalo, Maksim Antonov, Renno Veinthal ja Simo-Pekka Hannula

Uuriti vaskmaatrikskomposiitide (edaspidi vaskkomposiitide) kulumiskindlust, kasutades määrdeta hõõrdekulumiskatset. Vaskkomposiitide valmistamiseks kasutati plasma-aktiveeritud paagutust (PECS). Uuritud materjalid kujutasid endast dispersselt armeeritud komposiite. Maatriks põhines jämestruktuursel (c-Cu), submikromeetrilise struktuuriga (sm-Cu) või nanostruktuursel vasel (nCu). Armeerimiseks kasutati kupriidi- (Cu_2O), alumiiniumoksiidi- (Al_2O_3), titaandiboriidi- (TiB_2) või teemandiosakesi. Võrdluseks kasutati PECS-i abil valmistatud maatriksi materjale (ilma armeeriva lisandita). "Kuul-tasapinnal"-meetodil läbi viidud tribokatsed näitasid, et hõõrdetegurit μ, komposiidi kulumiskindlust ja kulumise mehhanismi mõjutab oluliselt hõõrdepaari vastaspoole materjali valik. Olenevalt uuritava materjali koostisest ja komposiidi ning hõõrdepaari teise elemendi vahelisest vastasmõju iseloomust määrati μ väärtuseks kroomterasest kuuli korral 0,71–1,01, kusjuures kulumine oli suur ($1{,}3 \times 10^{-5}$–$5{,}7 \times 10^{-3}$ mm^3/Nm). Väikseim hõõrdetegur ja kulumine saadi kupriidiga armeeritud vaskkomposiidi korral, kusjuures kulumine toimus oksüdatiivse ning abrasiivkulumise mehhanismi järgi. Alumiiniumoksiidi ja teemandiga armeeritud komposiitide korral täheldati adhesioonkulumist, kusjuures kulumise kiirus oli eelmistega võrreldes suurem. Leiti, et alumiiniumoksiidist kuuli korral on hõõrdetegur tunduvalt madalam (μ = 0,39–0,92) ja kulumine aeglasem ($1{,}4 \times 10^{-7}$–$6{,}1 \times 10^{-6}$ mm^3/Nm), kusjuures kulumisel täheldati oksüdatiivset iseloomu ning materjali kuhjumist kulumistsoonis. Materjalide võrdluses olid vastu Al_2O_3-kuuli madalaima hõõrdeteguriga Cu_2O- ja teemantarmatuuriga (5 nm) komposiidid, suurim kulumiskindlus saadi teemandiosakestega armeerimisel. Loodetavasti aitab käesolev töö materjalide, näiteks elektrotehnikas kasutatavate kontaktide materjalide valikul.